Accepted Article

Title: Cooperative Co(0)/Co(II) Sites Stabilized by a Perovskite Matrix Enable Selective C-O and C-C bond Hydrogenolysis of Oxygenated Arenes

Authors: Manish Shetty, Daniela Zanchet, William H Green, and Yuriy Román-Leshkov

A Journal of

ChemPubSoc
Europe

COMMUNICATION

Cooperative Co^0/Co^{II} Sites Stabilized by a Perovskite Matrix Enable Selective C-O and C-C bond Hydrogenolysis of Oxygenated Arenes

Manish Shetty[a], Daniela Zanchet[a],[b], William H. Green[a] and Yuriy Román-Leshkov*[a]

Abstract: A strontium (Sr)-substituted lanthanum cobaltite (La$_{0.8}$Sr$_{0.2}$CoO$_3$) matrix stabilized Co^0/Co^{II} catalytic sites that featured tunable C-O and C-C hydrogenolysis activity for the vapor-phase upgrading of oxygenated arenes. Co^{II} sites associated with oxygen vacancies were favored at low temperatures and performed selective C-O hydrogenolysis where Sr-substitution facilitated oxygen vacancy formation and led to ~10 times higher reactivity compared to undoped LaCoO$_3$. Co^0 sites were favored at high temperatures and performed extensive C-C bond hydrogenolysis generating a wide range of alkanes. The lower reaction order with P$_{H2}$ (1.1 ± 0.1) for C-C hydrogenolysis than for C-O hydrogenolysis (2.0 ± 0.1) led to high selectivity towards C-C hydrogenolysis at low P$_{H2}$. Given that Co$_3$O$_4$ surfaces featured a narrower temperature window for obtaining the respective optimal Co^{II} and Co^0 pairs compared to analogous perovskite surfaces, the perovskite matrix is implicated in stabilizing these pairs for selective C-O and C-C hydrogenolysis. This stabilization effect offers an additional handle to control reactivity in oxide catalysts.

Metal-metal oxide interfaces play a crucial role in governing C-O and C-C bond activation pathways.[1] These interfaces modulate the activity and product selectivity by influencing the adsorption and stabilization of intermediates, the availability of different active sites and the reaction mechanisms through structural and electronic effects.[2] In this respect, perovskite oxides (ABO$_3$), with their compositional diversity at the A and B sites offer ample opportunities to generate these interfaces that tune the oxygen mobility and redox properties of the catalyst.[3] These properties have been used in numerous catalytic applications, including volatile organic compound (VOC) elimination,[4] soot combustion,[5] selective oxidation of alkanes,[6] and NO$_x$ reduction.[7] Sr-substituted perovskites rivaled Pt-based commercial catalysts for NO$_x$ reduction under simulated diesel exhaust conditions.[7] They have also shown superior performance and tunability in electrochemical oxygen reduction and oxygen evolution reactions.[7-8] Most notably, recent studies have shown that under strongly reducing conditions, some late transition metals (e.g., Ni) in perovskites undergo exsolution, forming surface metallic clusters that are stabilized against agglomeration by the underlying perovskite matrix, thereby forming controlled metal-metal oxide interfaces.[9] Such interfaces provide oxygen vacancies for CO$_2$ activation and metal sites for C-C and C-H activation in the dry reforming of alkanes with

superior activity, remarkable stability and resistance to coking.[1d, 10]

In the context of renewable transportation fuels and chemicals, metal-metal oxide interfaces have been tailored to upgrade biomass-derived oxygenates via hydrogenolysis.[1a, 1c, 11] For instance, oxygen vacancies on metal oxide can work synergistically with metal sites to catalyze C-O bond hydrogenolysis, through enhanced H$_2$ activation on metal sites.[1a, 12] For ethanol steam reforming (ESR) on cobalt oxide, Co^0 sites catalyzed C-C bond cleavage, while the lattice oxide maintained catalyst stability through the removal of dehydrogenated fragments.[12-13] Surprisingly, despite their tremendous potential to generate tunable metal-metal oxides interfaces,[1d, 9, 14] perovskites have not been extensively studied as catalysts for C-O and C-C bond cleavage in biomass-derived oxygenates.

Herein, we investigated the Sr-substituted lanthanum cobaltite (La$_{0.8}$Sr$_{0.2}$CoO$_3$) catalyst for C-O and C-C hydrogenolysis of oxygenated arenes using coupled reactivity and characterization measurements. Specifically, we established the cooperative role of Co^{II} and Co^0 sites for C-O and C-C bond hydrogenolysis by studying the kinetics of C-C and C-O bond hydrogenolysis pathways during anisole conversion in combination with post-reaction X-ray photoelectron spectroscopy (XPS) and in situ powder X-ray diffraction (PXRD) coupled with temperature programed reduction (TPR). The role of Co^{II} sites for the C-O hydrogenolysis was further examined by considering the effect of Sr substitution on oxygen vacancy generation and comparing the C-O hydrogenolysis reactivity of La$_{0.8}$Sr$_{0.2}$CoO$_3$ and LaCoO$_3$. The reaction pathways for the hydrogenolysis products were mapped by studying the product selectivities with varying catalyst contact times and H$_2$O co-feed. Kinetic data for the reaction pathways was assembled into a kinetic model to gain mechanistic insight into the role of Co^0 and Co^{II} sites on the hydrogenolysis products. Overall, this study illustrates how the stabilization of interfacial Co^0 and Co^{II} sites can be used as a handle to control C-O and C-C hydrogenolysis activity.

Figure 1a shows the time-on-stream conversion profiles of anisole using La$_{0.8}$Sr$_{0.2}$CoO$_3$ in the temperature range between 473 and 623 K. At 473 K (P$_{H2}$ 1 bar), a 12 h transient induction zone was observed before reaching steady state at a conversion of 38%. At 523 K, the induction zone was significantly reduced, reaching a maximum conversion of 72% after ~1 h on stream. At this temperature, a conversion of 55% was measured after 18 h, consistent with a first-order deactivation rate constant of 0.02 h^{-1} (Figure S2). At higher temperatures (573 and 623 K), no induction zone was detected and the catalyst underwent a rapid initial deactivation (0.06 and 0.36 h^{-1} first order constants, respectively) achieving final conversions below 20%. The product selectivity values were invariant after ~5 h at all temperatures (Figure S3).

Product selectivity was a strong function of the reaction temperature (Figure 1b) and several reaction pathways were identified in the temperature range between 473 and 623 K, including C-O bond hydrogenolysis to benzene and methane, C-C bond hydrogenolysis to form C1-C6 alkanes, hydrogenation to form methoxycyclohexane and alkylation to form methyl anisole and toluene. The selectivity to benzene decreased from ~75% at 473 K to ~20% at 623 K with a concomitant increase in the selectivity to C1-C6 alkanes from ~5% at 473 K to ~70% at 623 K

[a]   Dr. M. Shetty, Prof. D. Zanchet, Prof. W.H. Green, Prof. Y Román-
      Leshkov
      Department of Chemical Engineering,
      Massachusetts Institute of Technology
      Cambridge, MA-02139 (USA)
      E-mail: yroman@mit.edu
[b]   Prof. D. Zanchet
      Institute of Chemistry, University of Campinas
      Campinas, SP-13083-970 (Brazil)
      Supporting information for this article is given via a link at the end of
      the document

COMMUNICATION

(see Figure S4 for product breakdown). The remaining products represented less than 5% at all temperatures. The increase of C-C bond hydrogenolysis products with temperature was expected, as the formation of metallic Co at high temperatures (*vide infra*) has been shown to favor the C-C bond cleavage reactions.[15] Interestingly, however, more than 80% of the hydrogenolysis products corresponded to methane at 523 K (Figure S4), suggesting strong adsorption of the reaction intermediates and complete C-C hydrogenolysis at the active sites. Control experiments using benzene as a feed at 523 K (Figure S5), showed complete C-C bond hydrogenolysis to form methane with low hydrogenation activity towards cyclohexane (~5%). Surprisingly, cyclohexane did not react under identical conditions.

Guaiacol exhibited similar reactivity trends to those of anisole at 523 K, with selectivity values approaching nearly constant values after ~5 h on stream (Figure S6). Both anisole and guaiacol exhibited selective $C_{aromatic}$-OCH$_3$ bond cleavage to form benzene and phenol, respectively (Table S2). The phenolic $C_{aromatic}$-OH bond was difficult to break in guaiacol as seen by the low selectivity towards benzene (~1.3%) and anisole (~1.6%). Guaiacol exhibited higher carbon accumulation rates (80% of total surface species) compared to anisole (50 % of total surface species) after 16 h on stream, as detected by XPS. As such, guaiacol conversion exhibited a higher deactivation rate (rate constant 0.07 h^{-1}) compared to anisole (0.02 h^{-1}), likely because of the faster accumulation of surface carbon (Figure S7).
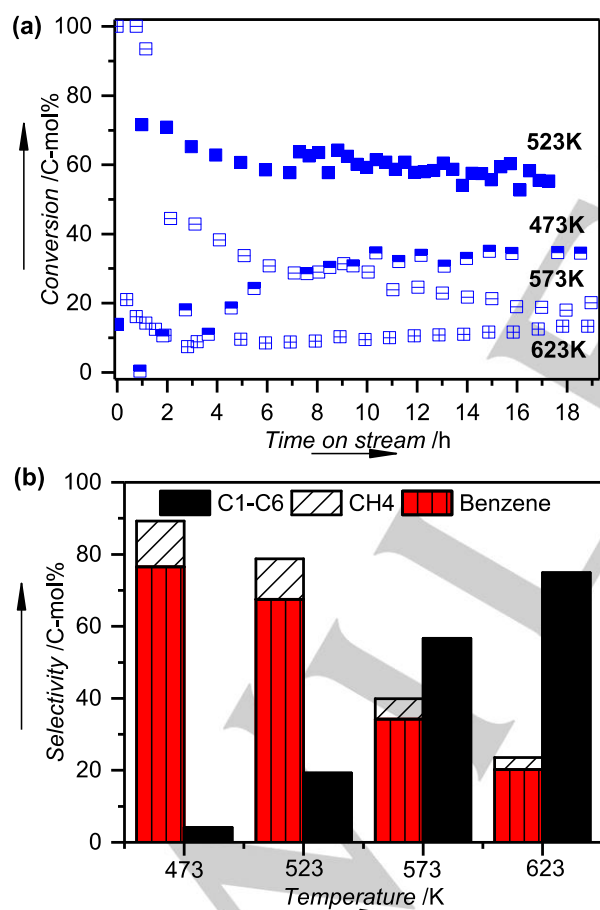

(a)

(b)

Figure 1. Reactivity of lanthanum strontium cobaltite (La$_{0.8}$Sr$_{0.2}$CoO$_3$) catalyst including (a) Conversion of anisole, and (b) Steady-state selectivity towards benzene and light gases (split as methane contribution from anisole HDO and other light gases) at 473. 623 K, 0.3-2.0 g La$_{0.8}$Sr$_{0.2}$CoO$_3$. Reaction conditions: P$_{Total}$ = 1.013 bar (P$_{Anisole}$ = 0.0098 bar, balance H$_2$).

To probe the reaction pathway from anisole, the conversion and selectivity of benzene were analyzed with varying catalyst contact times and P$_{H2O}$. The steady-state selectivity value to benzene was independent of the catalyst contact times spanning from 0.7 to 8.3 h (Figure 2a), implying parallel pathways for C-O and C-C bond hydrogenolysis reactions stemming from a common surface intermediate (Scheme S1). The addition of H$_2$O co-feed· known to competitively adsorb on active sites of metal oxides· at 523 K and ~9.5 h (Figure 2b) instantaneously reduced the conversion of anisole, but did not alter the product distribution. Upon removing H$_2$O at 14 h, the conversion increased again, reaching ~45% at 18 h. The reduction in anisole conversion in the presence of H$_2$O was not due to a shift in reaction equilibrium (see Table S3). We hypothesize that H$_2$O blocks the sites responsible for anisole adsorption, as also reported for steam reforming and CO oxidation.[16] Further, H$_2$O also inhibits the hydrogenolysis of benzene with no appreciable changes in selectivity (Figure S5). Taken together, we posit that the higher affinity of anisole to the perovskite surface favors its high surface coverage and inhibits the concerted C-C bond hydrogenolysis pathways of benzene.
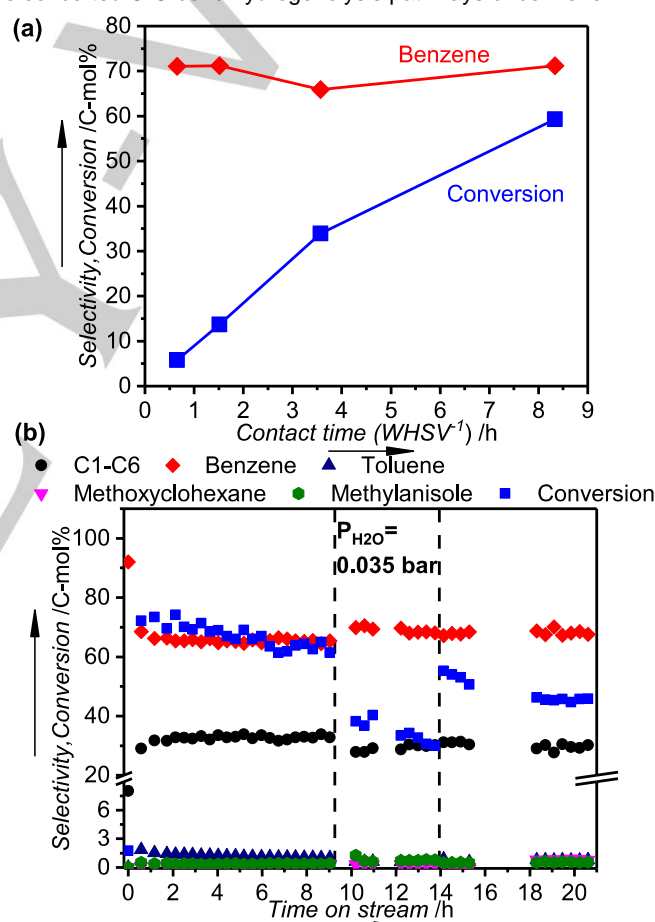

(a)

(b)

Figure 2. Reactivity of lanthanum strontium cobaltite (La$_{0.8}$Sr$_{0.2}$CoO$_3$) catalyst including (a) Selectivity towards benzene and conversion of anisole with varying catalyst contact times (1/WHSV) 0.7-8.3 h, 0.15-2.3 g La$_{0.8}$Sr$_{0.2}$CoO$_3$. (b) Conversion of anisole and selectivity of products during anisole HDO with and without H$_2$O as co-feed (P$_{H2O}$ = 0.035 bar). Reaction conditions: P$_{Total}$ = 1.013 bar (P$_{Anisole}$ = 0.0098 bar, balance H$_2$ without H$_2$O and P$_{Anisole}$ = 0.0098 bar, P$_{H2O}$ = 0.035 bar, balance H$_2$ with H$_2$O).

To shed light on genesis of reactivity on La$_{0.8}$Sr$_{0.2}$CoO$_3$, bulk and surface characterization were performed on the fresh and post-reaction catalysts (Figure 3). The PXRD pattern shows that the fresh La$_{0.8}$Sr$_{0.2}$CoO$_3$ was present in cubic structure.[17] The post-reaction catalysts showed that the material underwent lattice

COMMUNICATION

distortion, as indicated by the shift of the peaks at 2 = 23.5[0] and 48[0] to lower 2 values and splitting of the peaks at 33.5[0], 41[0] and 59[0]. These peak splittings have been attributed to octahedral tilting due to oxygen vacancy formation[18] and lattice expansion.[19] Interestingly, after exposure to air at room temperature, the PXRD pattern resembled the original pattern (Figure S9) suggesting that the lattice distortion under reaction condition is mostly reversed under oxidizing conditions.[20] Metallic Co was detected in the catalyst used at 623 K. H_2-TPR (Figure S8) showed that the reduction threshold of Co(III,IV) in $La_{0.8}Sr_{0.2}CoO_3$ was ~553 K, in agreement with the lattice distortion detected by in situ PXRD (Figure S10).

XPS was used to probe the changes in the catalyst surface composition post reaction. The Co $2p_{3/2}$ spectra (Figure 3b) shows that the fresh catalyst mainly featured Co(III,IV) species,[21] while after reaction, broader peaks appeared along with the satellite peak at ~785 eV (characteristic of octahedral Co[II] moieties). Thus, the Co species in the perovskite undergo partial reduction during reaction, consistent with the oxygen vacancy formation. At 623 K, the presence of Co[0] species at ~778 eV was detected, corresponding to ~8% Co[0] at the surface (Figure S11), in agreement with post-reaction PXRD. The O1s, La $3d_{5/2}$ and Sr 3d profiles did not exhibit any changes post-reaction (Figure S11).
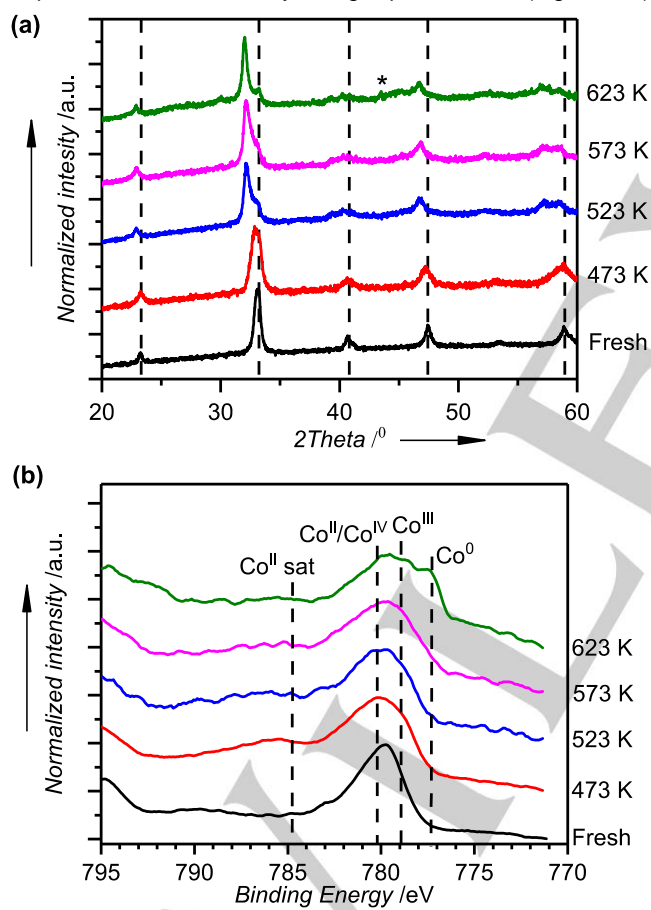

Figure 3. Post-reaction characterization of $La_{0.8}Sr_{0.2}CoO_3$ catalyst (a) PXRD pattern, and (b) XP spectra. Measurements performed at room temperature. The dashed lines in (a) corresponds to the main perovskite peaks (ICDD 04-018-5367) whereas the * indicates the (111) peak of metallic fcc Co (ICSD 622438). In (b), the dashed lines indicates the regions associated the different Co species.

The concomitant increase in the formation of Co[0] sites with the increase in deactivation rate of the catalyst, with reaction temperature (Figure S2) suggests that Co[II] sites are crucial for the

catalyst stability. In order to reinforce the role of Co[II] sites towards catalyst stability, anisole conversion was studied on cobalt oxide (Co_3O_4) catalyst under similar reaction conditions. At 473 K, the induction zone of 3h can be associated with the conversion of Co_3O_4 to CoO (Figures S14 and S16). At 523 and 573 K, the catalyst exhibited a higher deactivation rate (first-order constant 0.08 and 0.10 h^{-1}, respectively in Figure S15) than $La_{0.8}Sr_{0.2}CoO_3$, which is likely associated with the formation of Co metal (Figure S16). At 623 K, Co_3O_4 completely converted into Co metal and lost all catalytic activity (Figures S14 and S16) in stark contrast to $La_{0.8}Sr_{0.2}CoO_3$, which still exhibited metal-vacancy pairs at 623 K.

The role of Co[II] sites (oxygen vacancies) towards C-O hydrogenolysis, reactivity was further examined by comparing the rates for anisole conversion to benzene on $La_{0.8}Sr_{0.2}CoO_3$ and $LaCoO_3$ (Table S5) at 523 K. Mefford et al. reported a ~0.5 eV decrease in oxygen vacancy formation energy with Sr substitution from $LaCoO_3$ to $La_{0.75}Sr_{0.25}CoO_3$.[8] For C-O hydrogenolysis on oxides following a reverse Mars-van-Krevelen mechanism, this effect should lead to a higher reactivity.[1a, 8] Indeed, $La_{0.8}Sr_{0.2}CoO_3$ exhibited both specific and areal reaction rates an order of magnitude larger than unsubstituted $LaCoO_3$. These results strongly suggest the involvement of Co[II] sites for C-O bond hydrogenolysis, although other parameters such as surface composition and crystallinity can also contribute to the superior performance.[22]

The hydrogenation relative to hydrogenolysis of benzene on metals has been suggested to be related to its adsorption modes.[23] While hydrogenation may proceed through a weakly bound π-bonded intermediate, the hydrogenolysis is promoted by a strong chemisorption involving multiple metal-carbon bonds.[23b] On a perovskite surface, we propose that an oxygenate adsorbs on an oxygen vacancy (Scheme 1). The level of hydrogenolysis likely depends on the prevalence of the Co[0] sites and the resulting $Co-C_{Aromatic}$ bonds. With an increase in temperature, larger concentration of surface Co[0] sites are formed that promote C-C hydrogenolysis reactivity.[21, 24] Notably, the perovskite matrix appears to maximize such metal-vacancy pairs over a wider temperature range than what could be obtained with a regular monometallic oxide, as shown earlier.
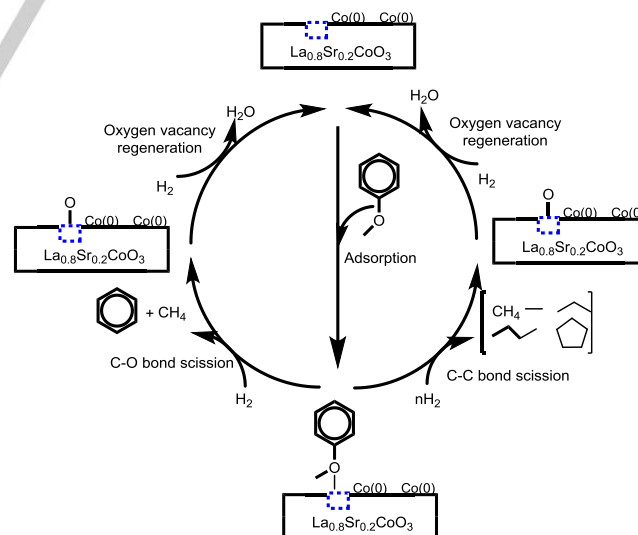
Scheme 1. Proposed pathways for anisole conversion on $La_{0.8}Sr_{0.2}CoO_3$ catalyst surface. Anisole adsorbs on the catalyst surface on an oxygen vacancy (represented by empty box) and the aromatic carbon atoms are associated with an ensemble of metallic Co[0] (represented as Co(0)) moieties.

In order to probe the reaction mechanism for anisole conversion, we examined the reaction kinetics of C-O and C-C bond hydrogenolysis from anisole at 523 K. As shown in Figure

COMMUNICATION

4, both C-O and C-C hydrogenolysis rates exhibit zero order with varying $P_{Anisole}$ suggesting saturation of anisole intermediates on oxygen vacancies. Specifically with respect to P_{H2}, the formation of C-O and C-C hydrogenolysis products show reaction order of 2.0 ± 0.1 and 1.1 ± 0.1, respectively. Due to the lower reaction order for C-C hydrogenolysis than C-O, a deleterious increased selectivity to C-C hydrogenolysis products against benzene (Figure S18) was observed with decreasing P_{H2} (~8% to ~57% as P_{H2} was decreased from 2.0 to 0.1 bar).

The observed reaction orders are consistent with a mechanistic model of anisole adsorption and its conversion to benzene on an oxygen vacancy (Co^{II} sites). With the participation of Co^0 sites in close proximity to Co^{II} sites, the adsorbed anisole can also undergo a sequence of hydrogenation and dehydrogenation steps to form H-deficient intermediates. The proposed mechanism (detailed in Supplementary Note 1) shows that the H content of equilibrated surface species leading to C-C hydrogenolysis requires H addition to achieve appreciable coverage of active surface species that undergo C-C bond cleavage, consistent with the positive reaction order with P_{H2}.[25]
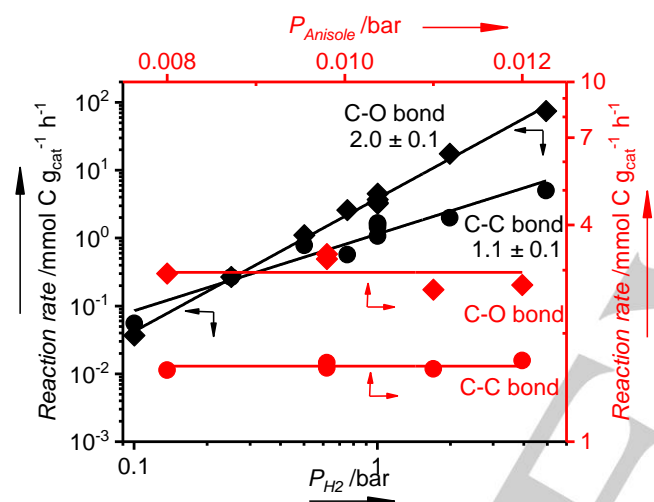

Figure 4. Reaction rate of C-O and C-C hydrogenolysis products from anisole with varying $P_{Anisole}$ (0.008-0.012 bar) and P_{H2} (0.1-5 bar) on lanthanum strontium cobaltite ($La_{0.8}Sr_{0.2}CoO_3$) catalyst (0.1-2.35 g) at 523 K. Reaction conditions: P_{Total} = 1.013 bar at P_{H2} and $P_{Total} - P_{H2}$. N_2 was used as a balance gas when P_{H2} < 1.0 bar.

Previous reports have studied the hydrogenation and hydrogenolysis of C_2-C_5 olefins and alkanes on $LaCoO_3$.[21, 24b, 26] With the aid of mechanistic analysis and tracer studies with D_2, it was deduced that the hydrogenolysis of olefins to form methane occurred through H deficient active surface species consistent with our hypothesis.[26b] In contrast to these reports, we do not observe any hydrogenolysis activity of alkanes. The stabilization of the bulk oxide lattice appeared to favor catalyst stability with the partial reduction of Co favoring hydrogenolysis and hydrogenation activity.[21, 27] Due to the catalyst deactivation with over-reduction to Co metal, Ichimura et al. attributed the hydrogenolysis activity to Co(III) moieties,[24b] while Ulla et al. attributed both the hydrogenation and hydrogenolysis activity to the presence of Co(0) moieties dispersed on the perovskite matrix[27b] consistent with our mechanistic model for C-C bond hydrogenolysis.

Overall, our results demonstrate the tunability of the C-O and C-C bond hydrogenolysis on perovskites with varying temperature and P_{H2}. While selective C-C hydrogenolysis was favored at high temperature and low P_{H2}, selective C-O hydrogenolysis can be achieved at low temperature and high P_{H2}. We also demonstrated the positive impact of Sr substitution on the C-O hydrogenolysis rates. Together with the possibility of

substituting other transition metals (e.g., Fe and Ni) in place of Co in $LaCoO_3$, our results clearly demonstrate new avenues for tuning the reactivity of perovskites and for developing highly active and selective catalysts under mild conditions.

Conflict of Interest

The authors declare no conflict of interest.

Keywords: b䕑{ æ•ⅆ}ç^¦•䕑}´ heterogeneous catalysis´ metal-metal oxide interfaces´ perovskite phases´ reaction mechanisms

References

[1] a) A. V. Mironenko, D. G. Vlachos, *J. Am. Chem. Soc.* **2016**, *138*, 8104-8113; b) S. Kattel, P. Liu, J. G. G. Chen, *J. Am. Chem. Soc.* **2017**, *139*, 9739-9754; c) X. Xiao, H. Bergstrom, R. Saenger, B. Johnson, R. Sun, A. Peterson, *Catal. Sci. Technol.* **2018**, *8*, 1819-1827; d) B. H. Zhao, B. H. Yan, S. Y. Yao, Z. H. Xie, Q. Y. Wu, R. Ran, D. Weng, C. Zhang, J. G. G. Chen, *J Catal* **2018**, *358*, 168-178; e) E. M. Anderson, M. L. Stone, M. J. Hulsey, G. T. Beckham, Y. Roman-Leshkov, *ACS Sustainable Chem Eng* **2018**, *6*, 7951-7959; f) K. Murugappan, E. M. Anderson, D. Teschner, T. E. Jones, K. Skorupska, Y. Roman-Leshkov, *Nat Catal* **2018**, *1*, 960-967.

[2] A. R. Puigdollers, P. Schlexer, S. Tosoni, G. Pacchioni, *ACS Catal.* **2017**, *7*, 6493-6513.

[3] S. Royer, D. Duprez, F. Can, X. Courtois, C. Batiot-Dupeyrat, S. Laassiri, H. Alamdari, *Chem. Rev.* **2014**, *114*, 10292-10368.

[4] N. Russo, D. Fino, G. Saracco, V. Specchia, *J Catal* **2005**, *229*, 459-469.

[5] J. R. Mawdsley, T. R. Krause, *Appl. Catal. A* **2008**, *334*, 311-320.

[6] C. H. Kim, G. S. Qi, K. Dahlberg, W. Li, *Science* **2010**, *327*, 1624-1627.

[7] J. Suntivich, H. A. Gasteiger, N. Yabuuchi, H. Nakanishi, J. B. Goodenough, Y. Shao-Horn, *Nat Chem* **2011**, *3*, 647-647.

[8] J. T. Mefford, X. Rong, A. M. Abakumov, W. G. Hardin, S. Dai, A. M. Kolpak, K. P. Johnston, K. J. Stevenson, *Nat Commun* **2016**, *7*, 11053.

[9] B. H. Zhao, B. H. Yan, Z. Jiang, S. Y. Yao, Z. Y. Liu, Q. Y. Wu, R. Ran, S. D. Senanayake, D. Weng, J. G. G. Chen, *Chem. Commun.* **2018**, *54*, 7354-7357.

[10] S. Singh, D. Zubenko, B. A. Rosen, *ACS Catal.* **2016**, *6*, 4199-4205.

[11] a) N. M. Briggs, L. Barrett, E. C. Wegener, L. V. Herrera, L. A. Gomez, J. T. Miller, S. P. Crossley, *Nat. Commun.* **2018**, *9*, 3827; b) E. M. Anderson, M. L. Stone, R. Katahira, M. Reed, G. T. Beckham, Y. Román-Leshkov, *Joule* **2017**, *1*, 613-622; c) M. L. Stone, E. M. Anderson, K. M. Meek, M. Reed, R. Katahira, F. Chen, R. A. Dixon, G. T. Beckham, Y. Roman-Leshkoy, *Acs Sustainable Chem Eng* **2018**, *6*, 11211-11218; d) M. Shetty, K. Murugappan, T. Prasomsri, W. H. Green, Y. Roman-Leshkov, *J. Catal.* **2015**, *331*, 86-97; e) M. Shetty, K. Murugappan, W.H. Green, Y. Roman-Leshkov, *ACS Sustainable Chem Eng* **2017**, *5*, 5293-5301.

COMMUNICATION

[12]   D. Zanchet, J. B. O. Santos, S. Damyanova, J. M. R. Gallo, J. M. C. Bueno, *Acs Catal* **2015**, *5*, 3841-3863.
[13]   C. Huck-Iriart, L. Soler, A. Casanovas, C. Marini, J. Prat, J. Llorca, C. Escudero, *Acs Catal* **2018**, *8*, 9625-9636.
[14]   M. Y. Chen, C. B. Chen, B. Zada, Y. Fu, *Green Chem* **2016**, *18*, 3858-3866.
[15]   T. R. Reina, E. Papadopoulou, S. Palma, S. Ivanova, M. A. Centeno, T. Ioannides, J. A. Odriozola, *Appl. Catal. B* **2014**, *150*, 554-563.
[16]   G. A. Martin, *J Catal* **1979**, *60*, 345-355.
[17]   M. Crespin, W. K. Hall, *J Catal* **1981**, *69*, 359-370.
[18]   S. Qin, A. I. Becerro, F. Seifert, J. Gottsmann, J. Z. Jiang, *J Mater Chem* **2000**, *10*, 2401-2401.
[19]   A. Y. Zuev, A. I. Vylkov, A. N. Petrov, D. S. Tsvetkov, *Solid State Ionics* **2008**, *179*, 1876-1879.
[20]   J. H. Kim, *Appl Surf Sci* **2011**, *258*, 350-355.
[21]   M. A. Ulla, E. A. Lombardo, *Bull. Chem. Soc. Jpn.* **1982**, *55*, 2311-2312.
[22]   X. Cheng, E. Fabbri, M. Nachtegaal, I. E. Castelli, M. El Kazzi, R. Haumont, N. Marzari, T. J. Schmidt, *Chem Mater* **2015**, *27*, 7662-7672.
[23]   a) P. H. Desai, J. T. Richardson, *J Catal* **1986**, *98*, 392-400; b) H. Kubicka, *J Catal* **1968**, *12*, 223-237.
[24]   a) J. Volter, M. Hermann, K. Heise, *J Catal* **1968**, *12*, 307-313; b) K. Ichimura, Y. Inoue, I. Yasumori, *Bull. Chem. Soc. Jpn.* **1982**, *55*, 2313-2314; c) J. H. Sinfelt, *Catal Lett* **1991**, *9*, 159-172.
[25]   D. W. Flaherty, E. Iglesia, *J. Am. Chem. Soc.* **2013**, *135*, 18586-18599.
[26]   a) K. Ichimura, Y. Inoue, I. Yasumori, *Bull. Chem. Soc. Jpn.* **1980**, *53*, 3044-3049; b) K. Ichimura, Y. Inoue, I. Yasumori, *Bull. Chem. Soc. Jpn.* **1981**, *54*, 1787-1792.
[27]   a) J. O. Petunchi, J. L. Nicastro, E. A. Lombardo, *J. Chem. Soc. Chem. Commun.* **1980**, 467-468; b) J. O. Petunchi, M. A. Ulla, J. A. Marcos, E. A. Lombardo, *J Catal* **1981**, *70*, 356-363.

WILEY-VCH

COMMUNICATION

Strontium-substituted lanthanum cobaltite ($La_{0.8}Sr_{0.2}CoO_3$) stabilizes Co^0/Co^{II} pairs to enable tunable C-O and C-C bond hydrogenolysis of lignin-derived oxygenated arenes.
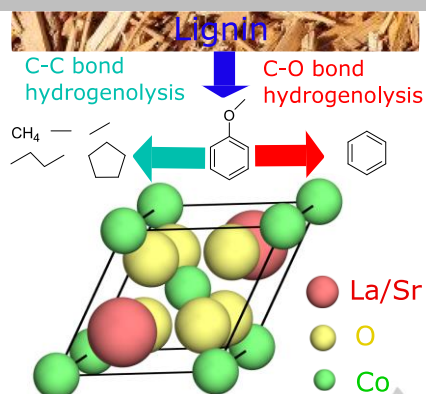
Manish Shetty, Daniela Zanchet, William H. Green and Yuriy Román-Leshkov

Page No. – Page No.

Cooperative Co^0/Co^{II} sites stabilized by a perovskite matrix enable selective C-O and C-C bond hydrogenolysis of oxygenated arenes